

Periodic Array of Complementary Artificial Magnetic Conductor MTMs-Based Multiband Antennas for Broadband Wireless Transceivers

Abstract— This paper presents the empirical results of a low-profile light-weight antenna based on a periodic array of the complementary artificial magnetic conductor metamaterial structure, which is realized by loading the antenna with E-shaped slits and inductive microstrip lines grounded using metallic via-holes. The finalized prototype antenna operates over a broadband of 0.41 – 4.1 GHz, which corresponds to a fractional bandwidth of 165.84%, and has dimensions of $40 \times 35 \times 1.6 \text{ mm}^3$ or $0.054\lambda_0 \times 0.047\lambda_0 \times 0.0021\lambda_0$, where λ_0 is free space wavelength at operating frequency of 410 MHz. The finalized antenna has a peak gain and radiation efficiency of 4.45 dBi and 85.8%, respectively, at 2.76 GHz. At the lower operating frequency of 410 MHz the gain and radiation efficiency are 1.05 dBi and 32.5%, respectively, which is normally highly challenging to realize with very small antennas. The planar nature of antenna enables easy integration with wireless transceivers.

Keywords— Planar antennas, multiband antennas, periodic array of complementary artificial magnetic conductor (CAMA), metamaterials (MTMs), broadband wireless transceivers.

I. INTRODUCTION

Rapid development of wireless communication systems is bringing about a wave of new wireless devices and systems to meet the demands of multimedia applications [1]–[2]. Multi-frequency and multi-mode devices such as cellular phones, wireless local area networks (WLANs) and wireless personal area networks (WPANs) place several demands on the antennas [3]–[4]. Primarily, the antennas need to have high gain, small physical size, broad bandwidth, versatility, embedded installation, etc. In particular, the impedance bandwidth, radiation patterns, gains and efficiencies are the most important factors that affect the application of antennas in contemporary and future wireless communication systems [5].

Research into metamaterials based on periodic unit-cells has grown rapidly with the discovery of left-handed metamaterials [6]–[7]. The transmission-line metamaterial (TL-MTM) technology has been applied to various types of antennas, i.e. compact antennas [8]–[12], leaky-wave antennas [13], and series-fed

antenna arrays [14]. In [7] the bandwidth and radiation characteristics of monopole antennas, which are based on T- and F-shaped radiators, are loaded with split-ring resonators of various sizes. In [9]-[12], the antenna designs are based on composite right/left-handed transmission-line unit-cells implemented by engraving slits on the radiating patch that is loaded with spiral inductors. This technology brings enabling capabilities, in particular: (i) the ability to strongly manipulate the propagation of EM-waves in confined small structure; and (ii) the freedom to precisely and systematically determine a broad set of parameters including the bandwidth, gain, efficiency, and physical size. Therefore, TL-MTMs appear to be a suitable candidate for developing electrically small antennas for multiband applications.

In this paper, a new artificial magnetic conductor (AMC) structure has been proposed for a low-profile antenna that offers enhanced gain performance, reduced back-lobe level radiation, wideband operation, and small physical footprint. The ground-plane of the antenna acts like a reflector for the radiation impinging on its surface; however the phase of radiation impinging on conductor's surface is reversed which can interfere destructively with the radiated waves from the antenna. This can significantly reduce the antenna's radiation efficiency. But if the reflected radiation is in-phase (i.e. 0°) or with phase change in the range $\pm 90^\circ$, then there will be a constructive interference of reflected wave with the radiated wave. This feature is exploited in this paper to improve the radiation characteristics of the antenna over its operating frequency range where the incoming radiations are reflected at angle between $\pm 90^\circ$. To accomplish this, the ground-plane of the proposed antenna is loaded with periodic array of E-shaped complementary artificial magnetic conductors (CAMC) and grounded inductive lines to realize metamaterial properties. The work is organized as follows: Section II describes the design process of implementing the proposed antennas and presents the simulated and measured results of the prototype antennas. Finally, the work is concluded in Section III.

II. ARTIFICIAL MAGNETIC CONDUCTOR SURFACES

In the analysis the cross-section of the antenna structure in Fig. 1 is considered. A cavity is formed by the perfect electric conductor (PEC) ground-plane and a partially reflective surface (PRS) placed at a distance (h) as described in [15]. The PRS is assumed to be a homogeneous surface in the analysis. The antenna function can be described by following the paths of the waves undergoing multiple reflections inside the cavity. Phase shifts are introduced by the path length, the PEC and the reflection coefficient of the PRS. Following the paths of the direct and the reflected waves and taking into account the various phase shifts introduced to them, the resonance condition of the cavity can be easily derived. The PEC introduces a phase shift of π . The resonance condition can be easily derived by imposing the phase difference of the

transmitted waves to be zero. The PRS introduces a phase shift equal to the phase of its transmission coefficient, ϕ_T . If $\phi_2 - \phi_1$ is the phase difference between direct and reflected waves, the resonance condition is written as follows:

$$\phi_2 - \phi_1 = 2\phi_T - \frac{2\pi}{\lambda}2h - \pi = 2N\pi, \quad N = 0, 1, 2, \dots \quad (1)$$

This resonant cavity behaves as a perfect magnetic conductor (at normal incidence) since it reflects normal incident waves with zero phase shift. Consequently, placing a simple point source in close proximity to the PRS would result in constructive interference between direct and reflected waves at the cavity resonance.

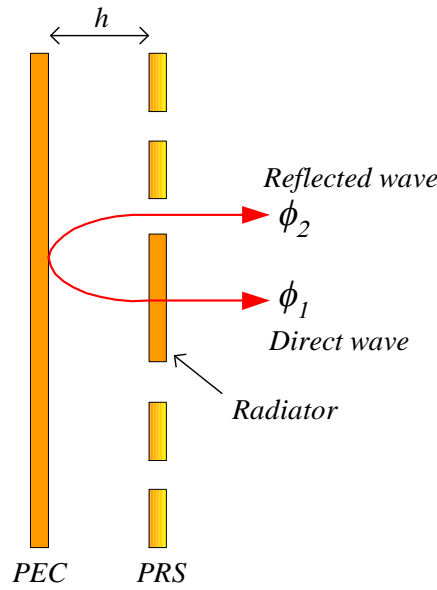


Fig. 1. Antenna cross-section where a resonant cavity is created by PEC and PRS.

A. Antenna #1

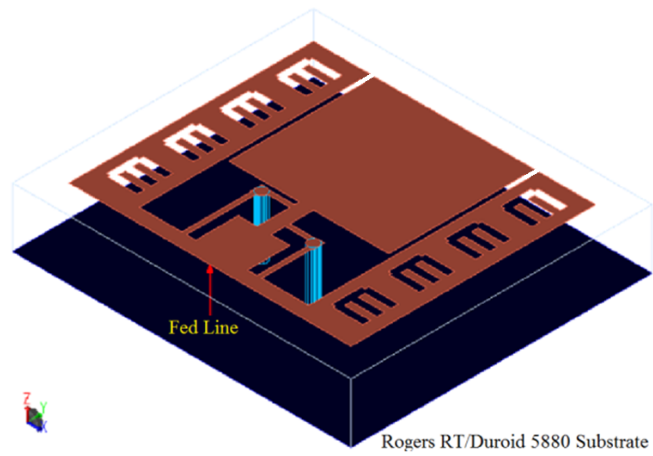
The geometry of Antenna #1 structure consists of two square radiation patches of different dimensions that are interconnected to each other with a microstrip-line. Two inverted L-shaped inductive lines are attached between the interconnecting line and the input feed-line plane, and are grounded at the bends using metallic via-holes to implement the shunt left-handed inductance that reflects the incident waves with reflection phase of near zero degrees. This proposed structure helps to enhance the antenna's impedance bandwidth and also determines the antenna's unidirectional radiation.

The E-shaped CAMC unit-cells create a resonance cavity in the antenna structure. As explained above the distance between the PEC and PRS must be such that the reflected waves through the PRS into space have equal phases in the normal direction. The resonance condition of the cavity is determined by Eqn. (1). The E-shaped CAMC unit-cells essentially concentrate the electromagnetic fields and currents near the

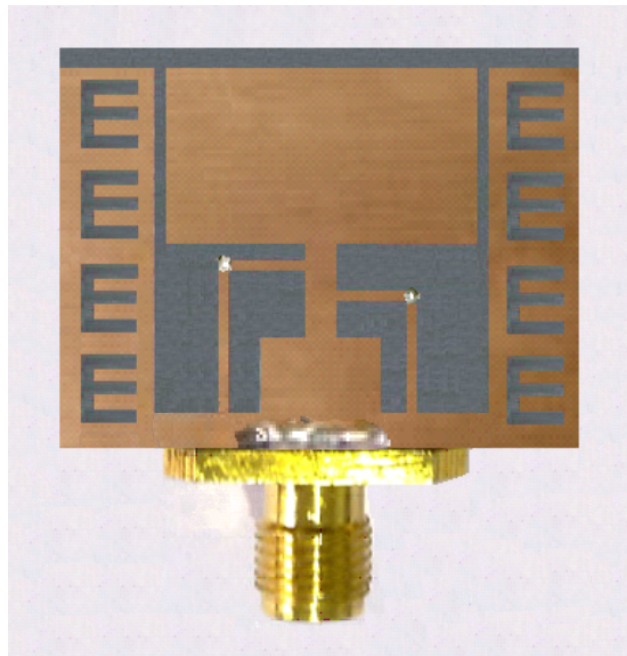
antenna structure to effectively prevent the fields from spreading along the antenna's ground plane and therefore contribute towards unwanted coupling. This technique should allow implementation of small antennas with minimal mutual coupling which is important to decorrelate multipath channels in small cellular systems.

Disposed on either side of the two square radiating patches are rectangular conductors that are loaded with periodic array of E-shaped slits, as shown in Fig. 2 (a). The slits act as complementary artificial magnetic conductor unit-cells exhibiting series left-handed capacitances [9]–[12]. Details of this technique are described in [16]–[17] where an AMC surface is created using square and rectangular loop slits. The AMC surfaces exhibit high surface impedance, due to which the magnetic field tangential to the surface vanishes. Hence, the structure reflects incident waves with zero or near zero phase shift. The proposed antenna is excited through an SMA connector located at the lower end of the smaller square patch. The CAMCs unit-cells produce fringing fields that make the effective dimensions of the patch greater than its physical dimensions. The size and number of CAMC unit-cells were determined through optimization using 3D full-wave electromagnetic simulator so that CAMC reflects incoming radiations at zero degrees. The goal here was to design and implement the antenna within an area of 40 mm². It was necessary to optimize the antenna's performance in terms of its impedance bandwidth and radiation characteristics. The antenna is constructed on Rogers RT/Duroid 5880 substrate with a dielectric permittivity (ϵ_r) and loss tangent ($\tan\delta$) of 2.2 and 0.0009, respectively. The substrate has a height (h) of 1.6 mm. The dimensions of Antenna #1 are: $27 \times 35 \times 1.6$ mm³ or $0.036\lambda_0 \times 0.046\lambda_0 \times 0.0021\lambda_0$ in terms of free-space wavelength at 400 MHz.

Although the single E-shaped slit is a narrowband resonant structure the extension in the bandwidth is achieved by electromagnetically coupling multiple E-shaped slits, as shown in Fig. 2, which is analogous to cascading together several identical narrowband resonators [9]–[11]. The simulated and measured reflection-coefficient and VSWR response in Fig. 3 confirm the antenna exhibits an impedance bandwidth of 1.9 GHz from 0.4 – 2.3 GHz for $S_{11} < -10$ dB, and its measured VSWR < 2 between 0.4 – 3.0 GHz. The antenna resonates in its operating range at four distinct frequencies, i.e. 700 MHz, 1250 MHz, 1820 MHz and 2080 MHz. The proposed antenna operates over UHF, L- and S-bands. Simulations and measurements were carried out using HFSS software and Agilent N5224A vector network analyzer, respectively. The proposed antennas were fabricated using standard manufacturing techniques.

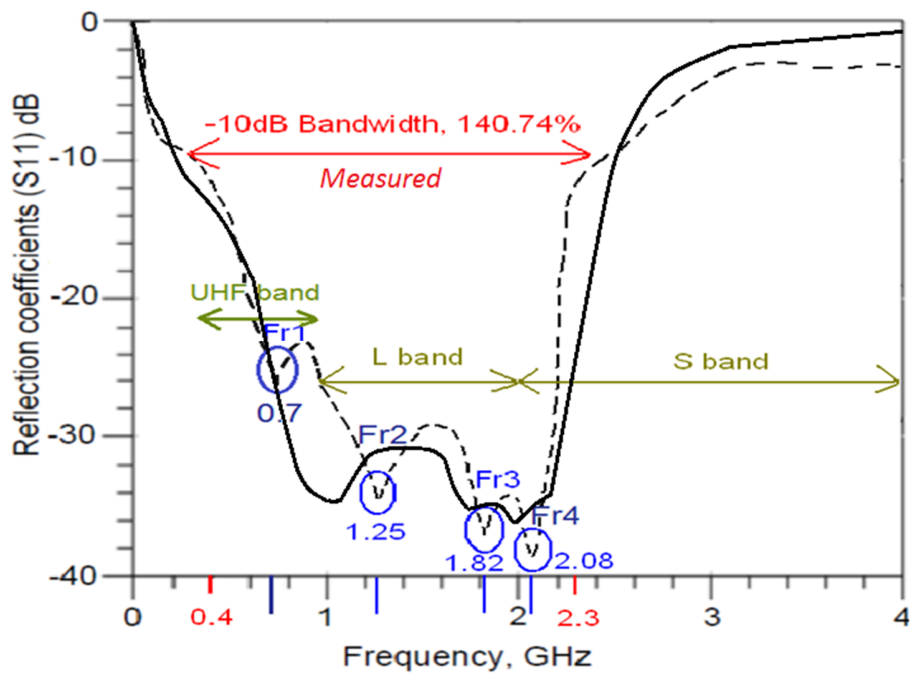


(a)

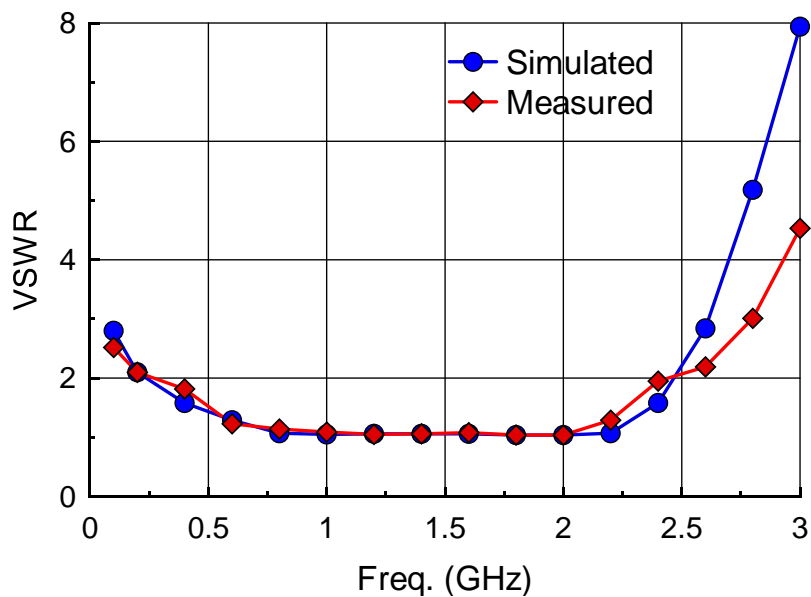


(b)

Fig. 2. (a) Perspective view of Antenna #1, and (b) fabricated prototype of Antenna #1. Dimensions are given in Table III.



(a) The simulated (solid line) and measured (dashed line) reflection-coefficient response.



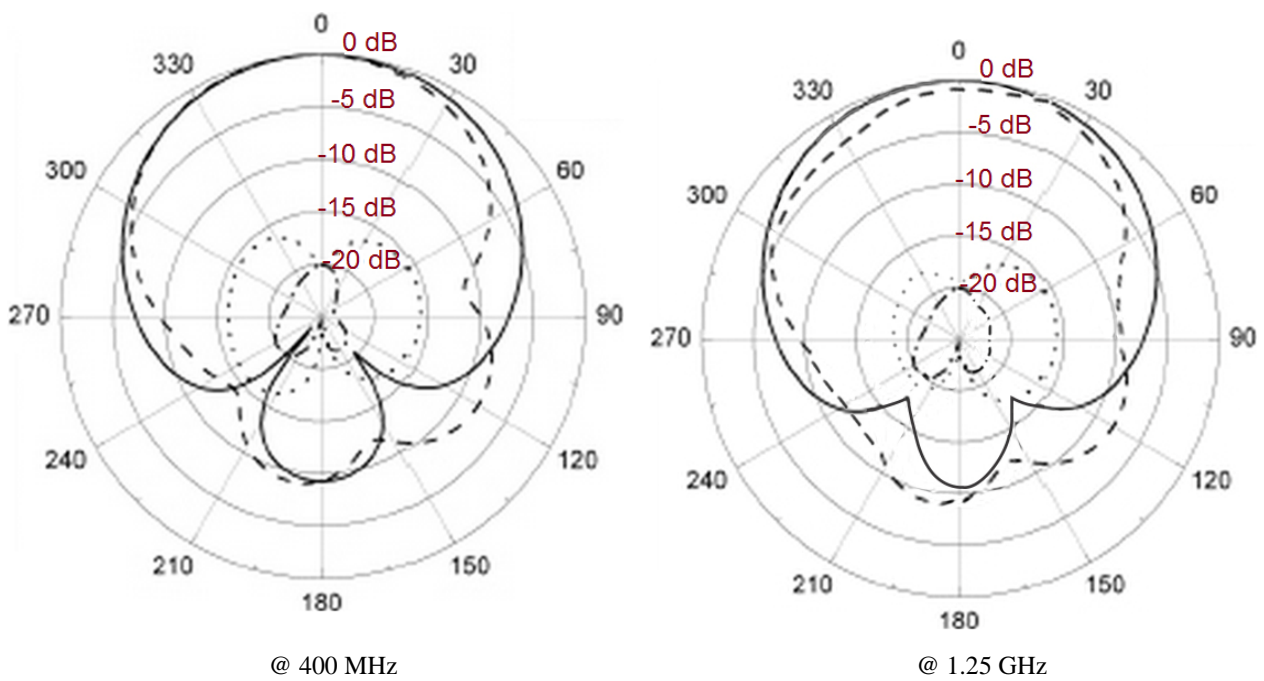
(b) The simulated (blue line) and measured (red line) voltage standing wave ratio response.

Fig. 3. The simulated and measured reflection-coefficient and VSWR of Antenna #1.

Agilent N5224A vector network analyzer used to characterize the antenna was calibrated with a standard short-open-load thru calibration procedure. The simulated and measured results presented agree well with each other showing the accuracy of the model is valid. The radiation pattern of the antenna was measured in a standard anechoic chamber. The antenna gain was measured using the comparative method that involves measuring the signal received by a reference antenna and by the antenna under test (AUT), and

determining the relative difference in the gain of both antennas when both the reference antenna and AUT are working in the received mode [18]. With this information, the gain of the test antenna is determined.

The measured radiation characteristics of the antenna at the different operating frequencies are shown in Fig. 4. The antenna radiates unidirectionally in both E- and H-planes. The cross-polarization is less than -20 dB for both planes, and the radiation characteristics essentially remain stable over the antenna's operating frequency range. The simulated and measured gain and radiation efficiency of Antenna #1 is shown in Fig. 5. It is evident that the measured gain and efficiency have a peak of 2.21 dBi and 51.4%, respectively, at the 4th resonant mode of 2.08 GHz. Salient features of the Antenna #1 are tabulated in Table I.



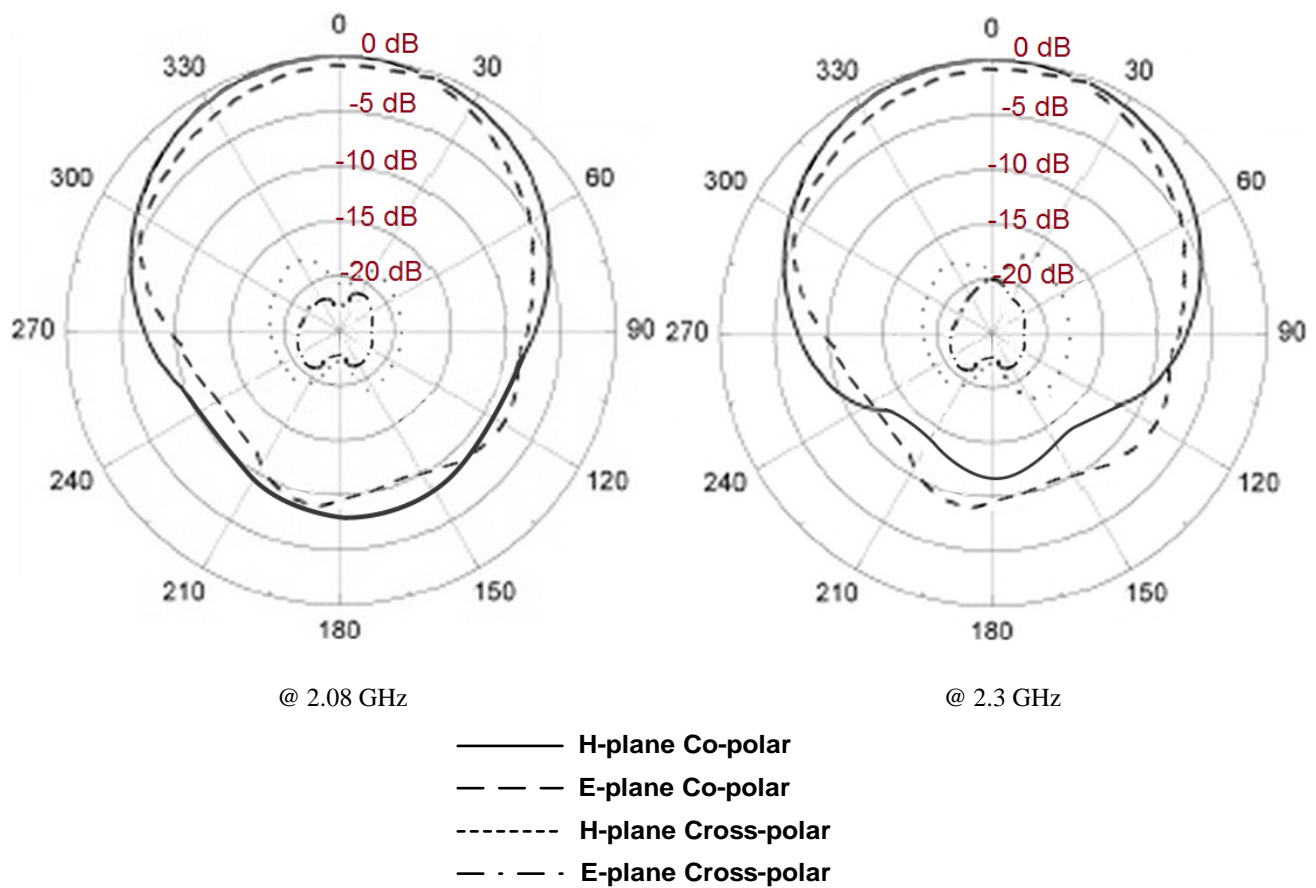


Fig. 4. Measured 2D radiation patterns of Antenna #1 at various operating frequencies of 0.4 GHz, 1.25 GHz, 2.08 GHz and 2.3 GHz.

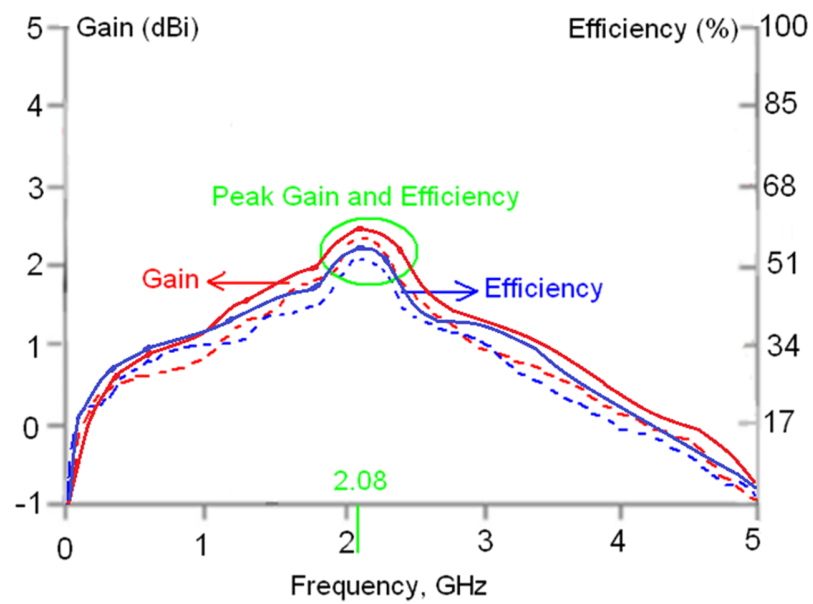


Fig. 5. The simulated (solid line) and measured (dashed line) gain and efficiency response of Antenna #1.

TABLE I. RADIATION CHARACTERISTICS OF ANTENNA #1

Frequency (GHz)		f_{start} : 0.4	f_{r1} : 0.7	f_{r2} : 1.25	f_{r3} : 1.82	f_{r4} : 2.08 (max)	f_{end} : 2.3
Simulated	Gain (dBi)	0.65	0.92	1.53	2.0	2.48	2.25
	Efficiency (%)	30.3	34.7	40.1	46.4	54.7	51.5
Measured	Gain (dBi)	0.5	0.73	1.2	1.88	2.21	2.0
	Efficiency (%)	28.7	31.1	37.3	44.9	51.4	49.6

B. Antenna #2

Besides the requirement of compact size, the proposed antenna needed to possess wide bandwidth and good radiation characteristics such as gain and efficiency performance. These characteristic features are conventionally achieved by increasing the effective cross-sectional area of antenna. The impedance bandwidth and radiation characteristics of the proposed antenna were improved by simply employing five additional E-shaped CAMC unit-cells that are located above the larger patch, as shown in Fig. 6, with the advantage of not affecting the radiating patch's physical dimensions. The impedance bandwidth and radiation characteristics of Antenna #2 are shown in Figs. 7-9. Antenna #2 has a size of $33 \times 35 \times 1.6 \text{ mm}^3$ or $0.047\lambda_0 \times 0.050\lambda_0 \times 0.0022\lambda_0$, where the free-space wavelength is 430 MHz.

The measured impedance bandwidth in Fig. 7 extends from 0.43 – 2.95 GHz for $S_{11} < -10 \text{ dB}$, which corresponds to 149.11%; thus covering UHF, L- and S-bands. The antenna has $VSWR < 2$ between 0.4 – 3.0 GHz. The antenna resonates in its operating range at the following frequencies: 0.75 GHz, 1 GHz, 1.25 GHz, 1.75 GHz, 2.05 GHz, 2.30 GHz, and 2.65 GHz. The antenna radiates unidirectionally in both E- and H-planes, as shown in Fig. 8, and its radiation characteristics are stable over the antenna's operating frequency range. Fig. 9 shows the antenna's simulated and measured gain and radiation efficiency performance have a peak value of 3.12 dBi and 52.7%, respectively, at the 6th resonant mode of 2.30 GHz. Salient features of the Antenna #2 are tabulated in Table II.

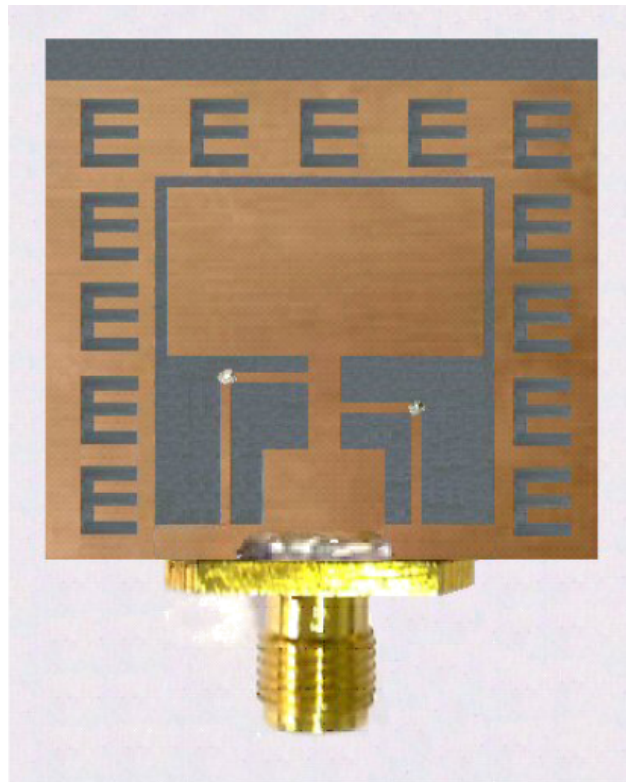
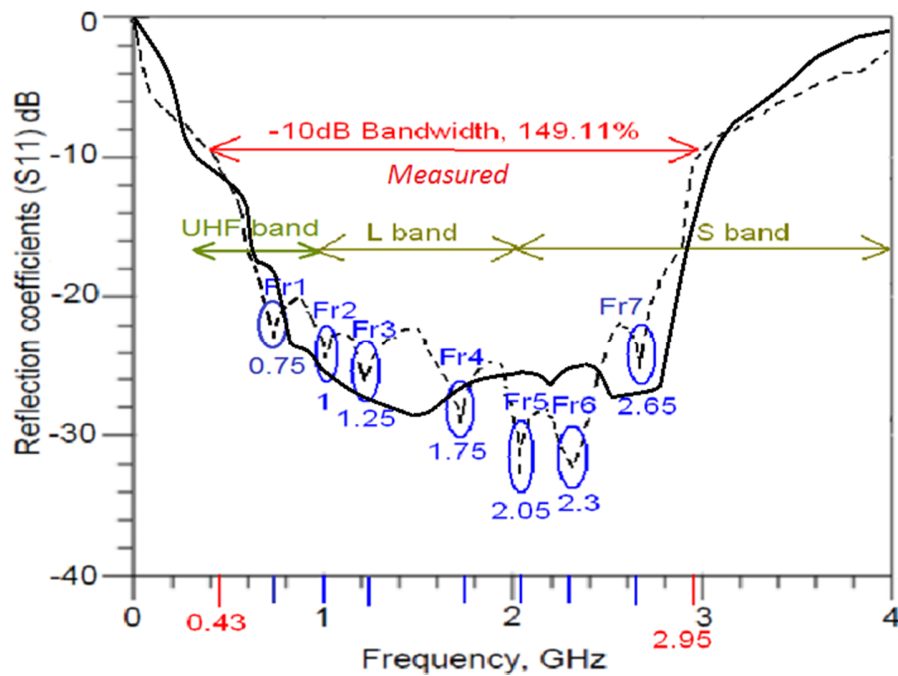
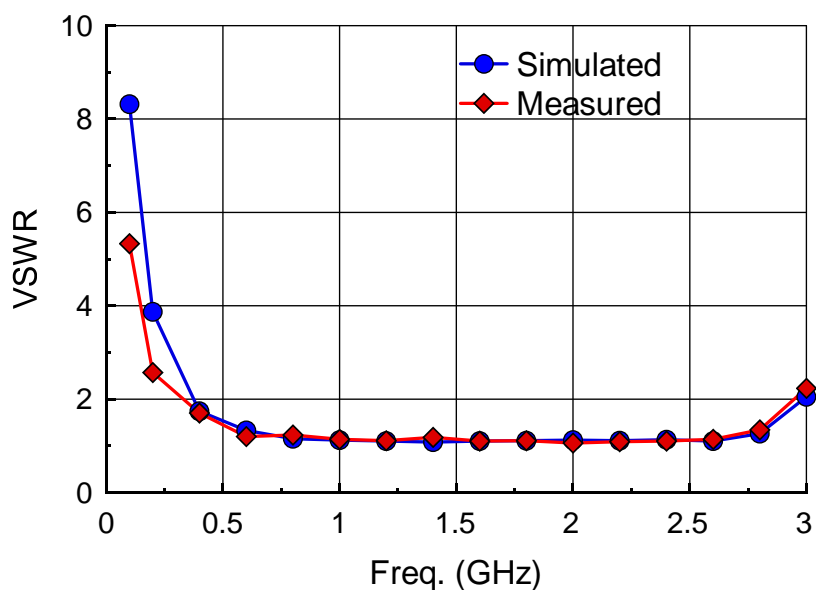


Fig. 6. Fabricated prototype of Antenna #2. Dimensions are given in Table III.

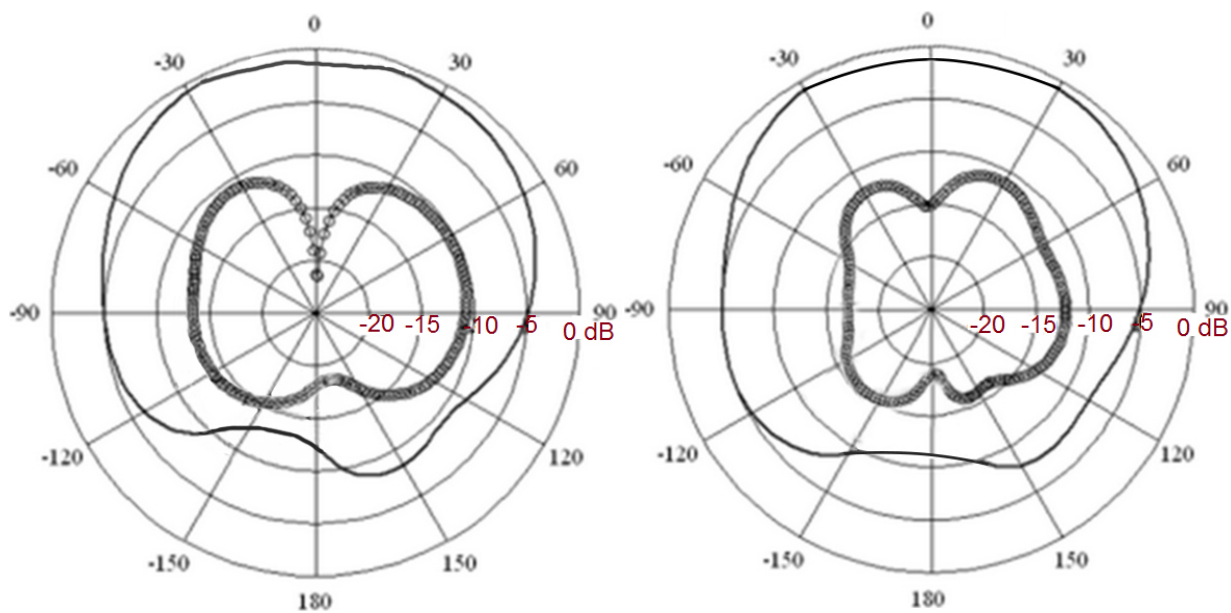


(a) The simulated (solid line) and measured (dashed line) reflection-coefficient response.



(b) The simulated (blue line) and measured (red line) voltage standing wave ratio response.

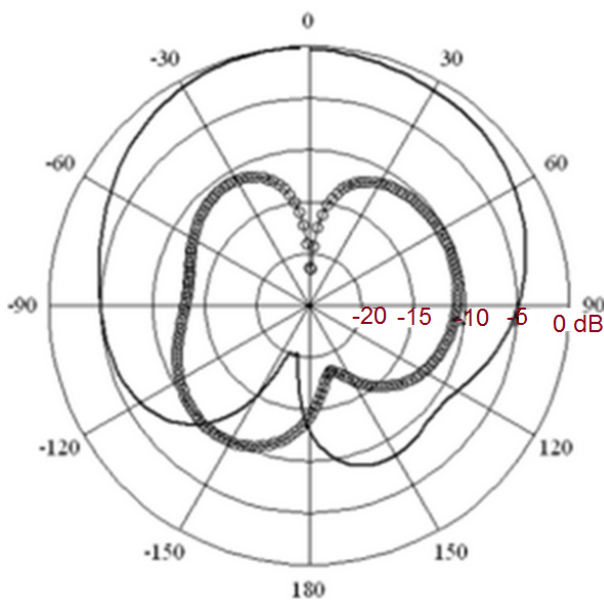
Fig. 7. The simulated and measured reflection-coefficients and VSWR of Antenna #2.



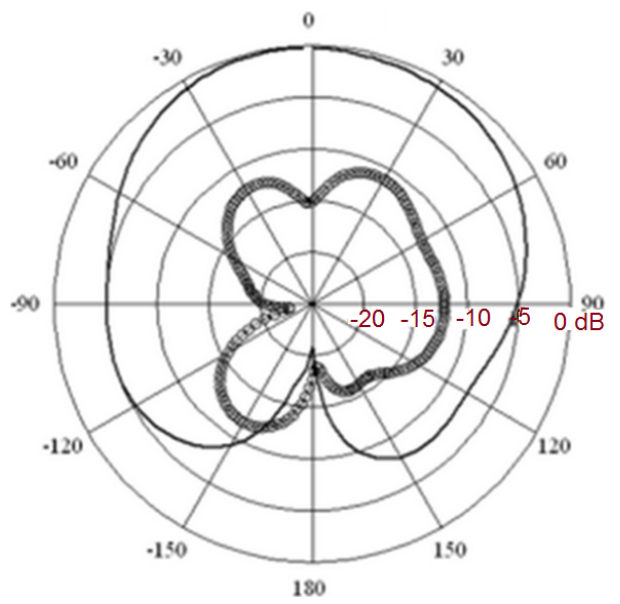
E-plane (faint line: Co-polar, and bold line: X-polar)

H-plane (faint line: Co-polar, and bold line: X-polar)

(a) @ 430 MHz

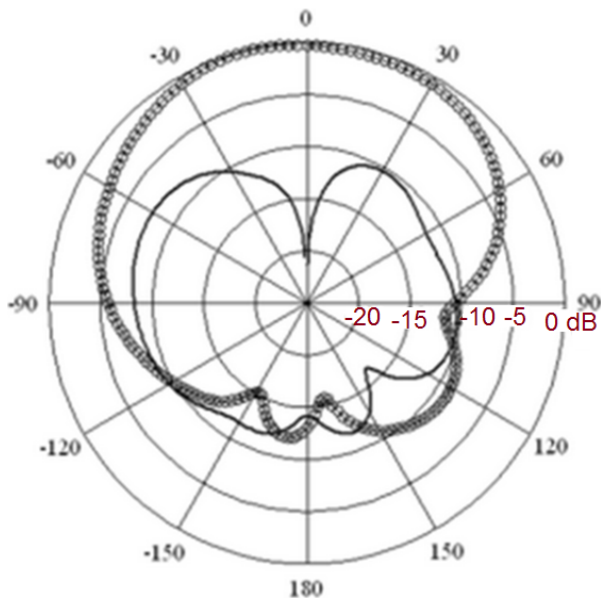


E-plane (faint line: Co-polar, and bold line: X-polar)

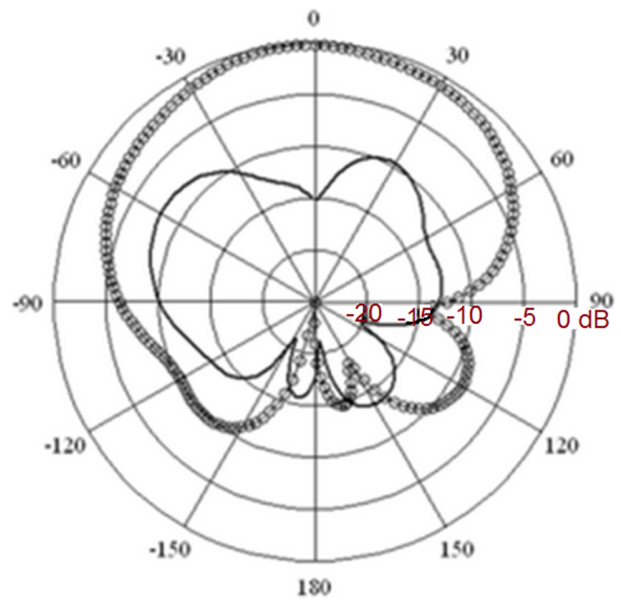


H-plane (faint line: Co-polar, and bold line: X-polar)

(b) @ 1 GHz

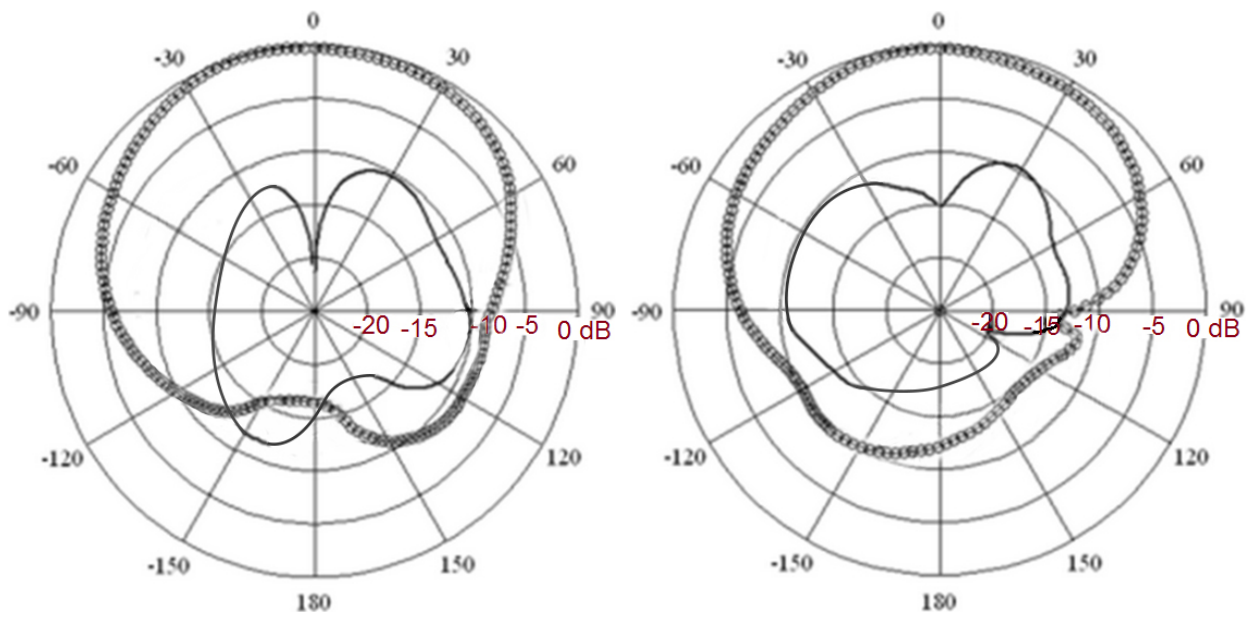


E-plane (bold line: Co-polar, and faint line: X-polar)



H-plane (bold line: Co-polar, and faint line: X-polar)

(c) @ 2.3 GHz



E-plane (bold line: Co-polar, and faint line: X-polar)

H-plane (bold line: Co-polar, and faint line: X-polar)

(d) @ 2.95 GHz

Fig. 8. Measured 2D radiation patterns of Antenna #2 at various operating frequencies of (a) 430 MHz, (b) 1 GHz, (c) 2.3 GHz, and (d) 2.95 GHz.

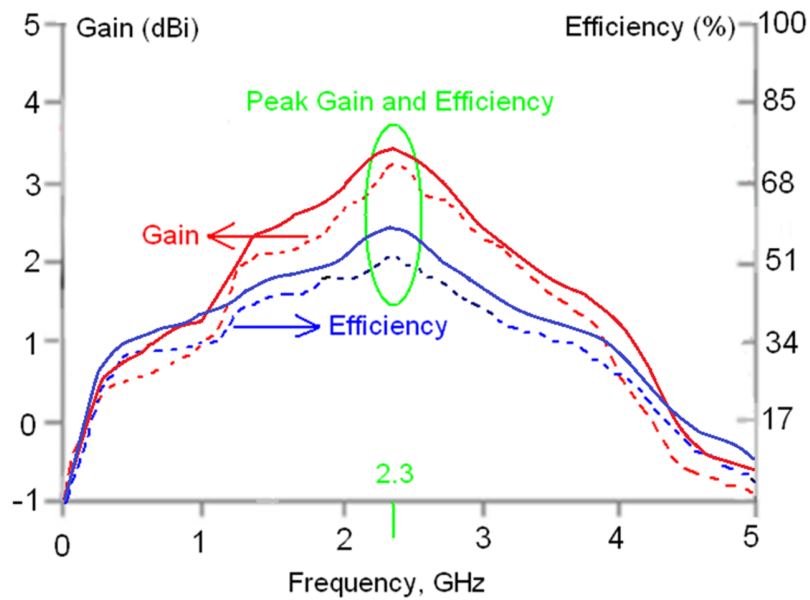


Fig. 9. The simulated (solid line) and measured (dashed line) gain and efficiency response of Antenna #2.

TABLE II. RADIATION CHARACTERISTICS OF ANTENNA #2

Frequency (GHz)		f_{start} : 0.43	f_{r1} : 0.75	f_{r2} : 1	f_{r3} : 1.25	f_{r4} : 1.75	f_{r5} : 2.05	f_{r6} : 2.3 (max)	f_{r7} : 2.65	f_{end} : 2.95
Simulated	Gain (dBi)	0.8	0.95	1.22	2.2	2.4	3.05	3.35	3.0	2.32
	Efficiency (%)	34.7	36.3	38.4	43.1	48.8	53.1	56.0	50.4	45.9
Measured	Gain (dBi)	0.65	0.8	1.0	2.0	2.28	2.75	3.12	2.86	2.15
	Efficiency (%)	32.0	33.2	34.5	40.7	44.3	48.5	52.7	47.1	39.8

C. Antenna #3

The next iteration is Antenna #3, which includes five additional E-shaped CAMCs unit-cells located above the larger square patch. Also included are two inductive lines connected to the larger patch at the lower edge to enhance the impedance bandwidth of the antenna. Ends of these inductive lines are connected to the ground-plane by the metallic via-holes, as shown in Fig. 10. Parameters defining Antenna #3 are labeled alphabetically in Fig. 10, and the corresponding values are given in Table III. The overall size of the antenna is $40 \times 35 \times 1.6 \text{ mm}^3$, which is equivalent to $0.054\lambda_0 \times 0.047\lambda_0 \times 0.0021\lambda_0$ at 410 MHz.

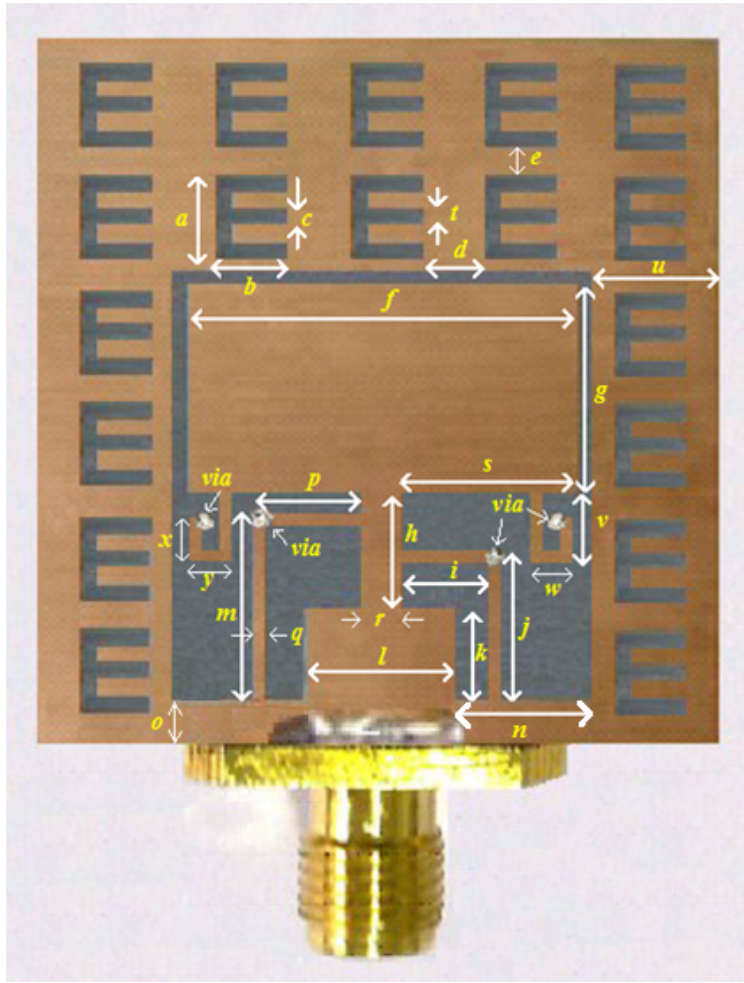


Fig. 10. Fabricated prototype of Antenna #3.

TABLE III. DIMENSIONS DEFINING THE PROPOSED ANTENNAS

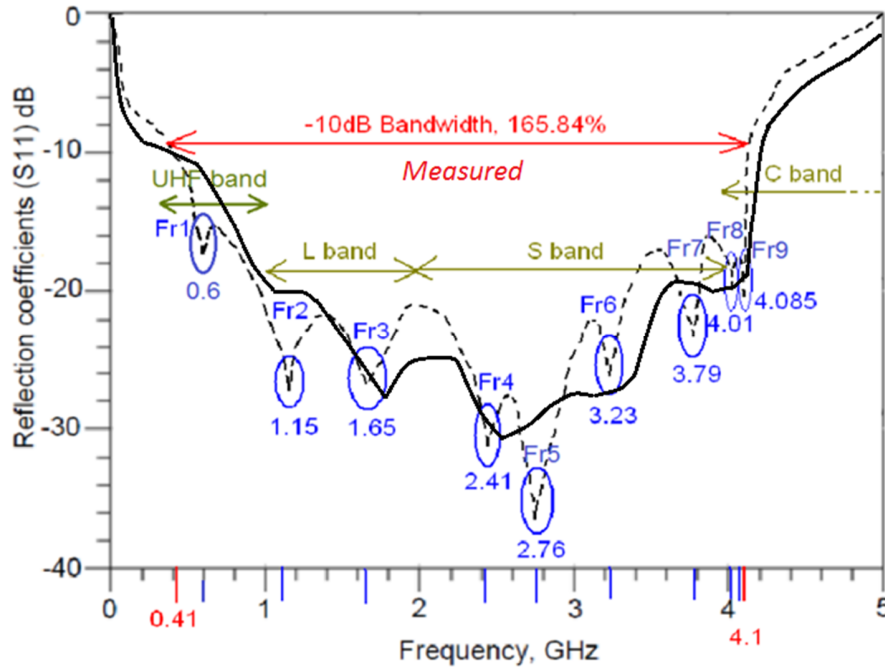
Parameters	<i>a</i>	<i>b</i>	<i>c</i>	<i>d</i>	<i>e</i>	<i>f</i>	<i>g</i>	<i>h</i>	<i>i</i>	<i>j</i>	<i>k</i>	<i>l</i>	<i>m</i>	<i>n</i>	<i>o</i>	<i>p</i>	<i>q</i>	<i>r</i>	<i>s</i>	<i>t</i>	<i>u</i>	<i>v</i>	<i>w</i>	<i>x</i>	<i>y</i>
Size (mm)	5	4	0.8	3	1.4	23	13	7.2	5.4	8.8	5.4	8.8	11.5	8	2.3	6.5	0.8	2.3	10.35	0.8	8.3	4.2	2.3	2.3	2.3

The simulated and measured reflection coefficient and VSWR response of Antenna #3 are shown in Fig. 11. The antenna has an experimental impedance bandwidth of 3.69 GHz from 0.41 – 4.1 GHz for $VSWR < 1.5$ that corresponds to a fractional bandwidth of 165.84%. Antenna #3 resonates in its operating range at 600 MHz, 1.15 GHz, 1.65 GHz, 2.41 GHz, 2.76 GHz, 3.23 GHz, 3.79 GHz, 4.01 GHz, and 4.085 GHz. The antenna is usefulness in the frequency range covering UHF to C- band.

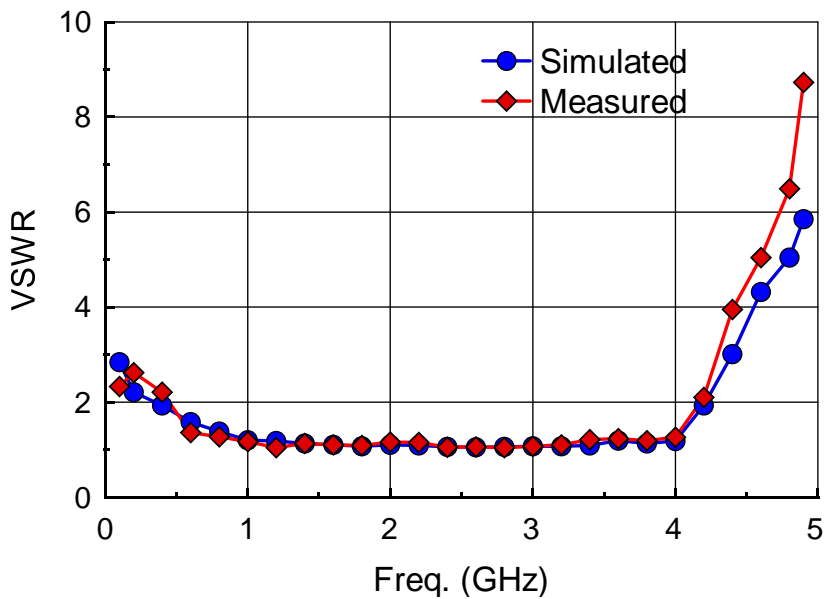
Also, since we have proposed a UWB antenna, the time domain characteristic like group delay, which is defined by (2), for help in justifying antenna for UWB applications is presented in Fig. 11 (c).

$$D(\omega) \triangleq -\frac{d\theta(\omega)}{d(\omega)}. \quad (2)$$

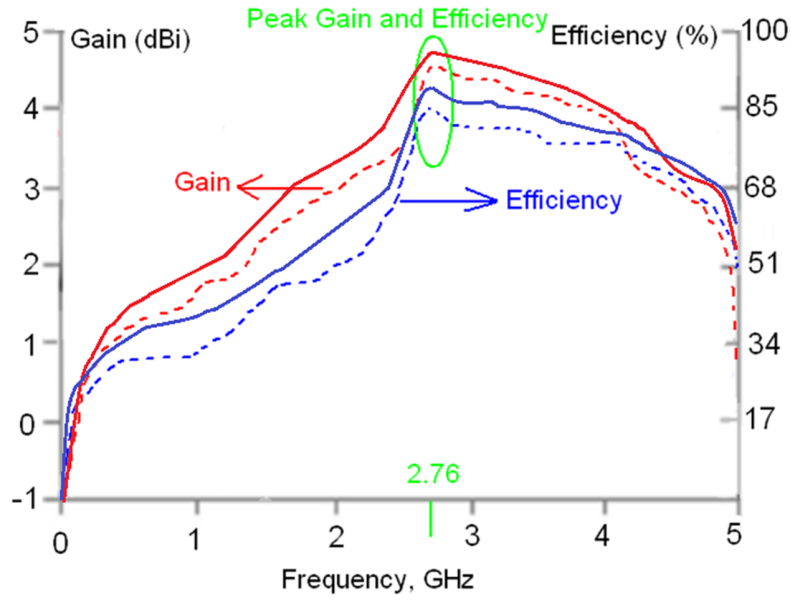
The antenna radiates unidirectionally in both E- and H-planes. The cross-polarization is less than -20 dB for both planes, and the radiation characteristics essentially remain constant over the antenna's operating frequency range, as shown in Fig. 11 (d).



(a) The simulated (solid line) and measured (dashed line) reflection-coefficient response.



(b) The simulated (blue line) and measured (red line) voltage standing wave ratio response.



(e) The simulated (solid line) and measured (dashed line) gain and efficiency response of Antenna #3.

Fig. 11. The simulated and measured reflection coefficient, VSWR, group delay diagram, 2D radiation patterns and gain and efficiency curves of Antenna #3.

The simulated and measured gain and radiation efficiency of Antenna #3 are shown in Fig. 11 (e). It is evident that the measured gain and efficiency performance have a peak value of 4.45 dBi and 85.8%, respectively, at the 5th resonant mode of 2.76 GHz. Salient features of the Antenna #3 are tabulated in Table IV.

TABLE IV. RADIATION CHARACTERISTICS OF ANTENNA #3

Frequency (GHz)		f_{start} :	f_{r1} :	f_{r2} :	f_{r3} :	f_{r4} :	f_{r5} : 2.76 (max)	f_{r6} :	f_{r7} :	f_{r8} :	f_{r9} :	f_{end} :
Simulated	Gain (dBi)	1.15	1.51	2.05	2.9	3.63	4.75	4.53	4.21	4.08	3.91	3.88
	Efficiency (%)	34.2	37.1	40.3	51.8	65.0	88.6	84.8	79.2	77.8	75.2	73.7
Measured	Gain (dBi)	1.05	1.35	1.85	2.65	3.41	4.45	4.21	4.0	3.88	3.79	3.7
	Efficiency (%)	32.1	33.4	36.8	48.3	62.9	85.8	80.2	76.6	74.5	73.4	72.4

The criteria used to determine the number CAMC unit-cells depend on a tradeoff between the antenna dimensions, impedance bandwidth, and radiation characteristics. The overall goal here was to design and implement an antenna that fitted within an area of 40 mm² and exhibited an ultra-wide bandwidth with good unidirectional radiation patterns. The number and size of unit-cells were determined through optimization using High Frequency Simulator Structure (HFSS). Figs. 3, 7 and 11 show the

reflection coefficients of the antennas with increasing number of CAMC unit-cells from 8 to 18. **Eighteen unit-cells provide the impedance bandwidth of 0.41GHz – 4.1GHz for a reflection-coefficient of -10 dB.** Therefore, eighteen unit-cells were used here in the final antenna design. Salient characteristics of the three antennas are summarized in Table V. It is evident that Antenna #3 when compared with Antenna #1 has significantly improved impedance bandwidth, gain and efficiency by 17.8%, 101.4%, and 66.9%, respectively. This is attributed to the ten CAMC unit-cells that extend the effective aperture of Antenna #3.

TABLE V. MEASURED PERFORMANCE OF THE PROPOSED ANTENNAS

Antenna #1	
Dimensions	$0.036\lambda_0 \times 0.046\lambda_0 \times 0.0021\lambda_0$ at 400 MHz or $27 \times 35 \times 1.6 \text{ mm}^3$
Fractional bandwidth	140.74% (400 MHz – 2.3 GHz)
Max. Gain (dBi)	2.21 @ $f_{r4} = 2.08 \text{ GHz}$
Max. Efficiency (%)	51.4 @ $f_{r4} = 2.08 \text{ GHz}$

Antenna #2	
Dimensions	$0.047\lambda_0 \times 0.050\lambda_0 \times 0.0022\lambda_0$ at 430 MHz or $33 \times 35 \times 1.6 \text{ mm}^3$
Fractional bandwidth	149.11% (430 MHz–2.95 GHz)
Max. Gain (dBi)	3.12 @ $f_{r6} = 2.3 \text{ GHz}$
Max. Efficiency (%)	52.7 @ $f_{r6} = 2.3 \text{ GHz}$

Antenna #3	
Dimensions	$0.054\lambda_0 \times 0.047\lambda_0 \times 0.0021\lambda_0$ at 410 MHz or $40 \times 35 \times 1.6 \text{ mm}^3$
Fractional bandwidth	165.84% (410 MHz–4.1 GHz)
Max. Gain (dBi)	4.45 @ $f_{r5} = 2.76 \text{ GHz}$
Max. Efficiency (%)	85.8 @ $f_{r5} = 2.76 \text{ GHz}$

The antenna efficiency was measured in an anechoic chamber by feeding power to the antenna feed and measuring the strength of the radiated electromagnetic field in the surrounding space. The efficiency was calculated by taking the ratio of the radiated power to the input power of the antenna. The gain of the antenna was measured using the standard gain comparison technique where pre-calibrated standard gain antenna was used to determine the absolute gain of the antenna under test.

To validate the design procedure, the proposed antennas specifications have compared with some of recent antennas in Table VI.

TABLE VI. SPECIFICATIONS OF THE PROPOSED ANTENNAS COMPARED WITH RECENT MULTIBAND AND BROADBAND ANTENNAS (UC: unit cells, ES: electrically size and PHS: physically size)

Papers	Dimensions	Bandwidth	Gain (Max)	Eff. (Max)
[7] F-ant. without SRR	ES: $0.063\lambda_0 \times 0.029\lambda_0 \times 0.002\lambda_0$ at 1 GHz PHS: $19 \times 8.8 \times 0.8 \text{ mm}^3$	4–5.5 GHz (31.5%)	3.6 dBi	78.5%
[7] T-ant. without SRR	ES: $0.063\lambda_0 \times 0.054\lambda_0 \times 0.002\lambda_0$ at 1 GHz PHS: $19 \times 16.2 \times 0.8 \text{ mm}^3$	3.82–5.8 GHz (41.16%)	3.9 dBi	80.2%
[7] F-ant. with SRR	ES: $0.01\lambda_0 \times 0.073\lambda_0 \times 0.002\lambda_0$ at 1 GHz PHS: $30 \times 22 \times 0.8 \text{ mm}^3$	2.9–6.41 GHz (75.4%)	4 dBi	81.2%
[7] T-ant. with SRR	ES: $0.01\lambda_0 \times 0.073\lambda_0 \times 0.002\lambda_0$ at 1 GHz PHS: $30 \times 22 \times 0.8 \text{ mm}^3$	2.6–6.6 GHz (~87%)	4.4 dBi	82.6%
[9]	ES: $0.068\lambda_0 \times 0.022\lambda_0 \times 0.002\lambda_0$ at 1 GHz PHS: $20.4 \times 6.8 \times 0.8 \text{ mm}^3$	5.8–7.3 GHz (23%)	4.8 dBi	78%
[10] 4 UC, L-antenna	ES: $0.044\lambda_0 \times 0.016\lambda_0 \times 0.002\lambda_0$ at 1 GHz PHS: $13.4 \times 4.9 \times 0.8 \text{ mm}^3$	0.2–1.8 GHz (160%)	3.4 dBi	88%
[10] 5 UC, F-antenna	ES: $0.048\lambda_0 \times 0.014\lambda_0 \times 0.005\lambda_0$ at 1 GHz PHS: $14.5 \times 4.4 \times 1.6 \text{ mm}^3$	0.11–2.1 GHz (180.1%)	4.5 dBi	95%
[11] 8 UC, J-antenna	ES: $0.075\lambda_0 \times 0.02\lambda_0 \times 0.027\lambda_0$ at 1 GHz PHS: $22.6 \times 7 \times 0.8 \text{ mm}^3$	7.25–17.8 GHz (84.23%)	2.3 dBi	48.2%
[11] 7 UC, I-antenna	ES: $0.072\lambda_0 \times 0.02\lambda_0 \times 0.005\lambda_0$ at 1 GHz PHS: $21.7 \times 7 \times 1.6 \text{ mm}^3$	7.8–19.85 GHz (87.16%)	3.4 dBi	68.1%
[11] 6 UC, J-antenna	ES: $0.06\lambda_0 \times 0.02\lambda_0 \times 0.027\lambda_0$ at 1 GHz PHS: $18 \times 7 \times 0.8 \text{ mm}^3$	7.5–16.8 GHz (74.4%)	2.1 dBi	44.3%
[11] 5 UC, I-antenna	ES: $0.056\lambda_0 \times 0.02\lambda_0 \times 0.005\lambda_0$ at 1 GHz PHS: $16.7 \times 7 \times 1.6 \text{ mm}^3$	7.7–18.6 GHz (82.88%)	3.1 dBi	58.6%
[12]	ES: $0.075\lambda_0 \times 0.019\lambda_0 \times 0.002\lambda_0$ at 1 GHz PHS: $22.6 \times 5.8 \times 0.8 \text{ mm}^3$	0.5–11.3 GHz (183%)	6.5 dBi	88%
[19]	ES: $0.2\lambda_0 \times 0.05\lambda_0 \times 0.003\lambda_0$ at 1 GHz PHS: $60 \times 16 \times 1 \text{ mm}^3$	0.67–2.55 GHz (116.7%)	4.74 dBi	62.88%
[20]	ES: $0.06\lambda_0 \times 0.06\lambda_0 \times 0.005\lambda_0$ at 1 GHz PHS: $18 \times 18 \times 1.6 \text{ mm}^3$	1.8–2.35 GHz (26.5%)	3.69 dBi	20%
[21]	ES: $0.2\lambda_0 \times 0.017\lambda_0 \times 0.017\lambda_0$ at 1 GHz PHS: $60 \times 5 \times 5 \text{ mm}^3$	0.8–2.5 GHz (103.03%)	0.45 dBi	53.6%
[22]	ES: $0.06\lambda_0 \times 0.06\lambda_0 \times 0.021\lambda_0$ at 1 GHz PHS: $18.2 \times 18.2 \times 6.5 \text{ mm}^3$	1–2 GHz, (66.66%)	0.6 dBi	26%
[23]	ES: $0.04\lambda_0 \times 0.04\lambda_0 \times 0.011\lambda_0$ at 1 GHz PHS: $12 \times 12 \times 3.33 \text{ mm}^3$	2.34–2.54 GHz, (8.2%)	1 dBi	22%
[24]	ES: $0.07\lambda_0 \times 0.08\lambda_0 \times 0.003\lambda_0$ at 1 GHz PHS: $20 \times 25 \times 0.8 \text{ mm}^3$	3.45–3.75 GHz, (8.33%)	2 dBi	27%
Proposed Antenna #1	ES: $0.090\lambda_0 \times 0.116\lambda_0 \times 0.005\lambda_0$ at 1 GHz PHS: $27 \times 35 \times 1.6 \text{ mm}^3$	0.4–2.3 GHz (140.74%)	2.21 dBi	51.4%
Proposed Antenna #2	ES: $0.110\lambda_0 \times 0.116\lambda_0 \times 0.005\lambda_0$ at 1 GHz PHS: $33 \times 35 \times 1.6 \text{ mm}^3$	0.43–2.95 GHz (149.11%)	3.12 dBi	52.7%

Proposed Antenna #3	ES: $0.133\lambda_0 \times 0.116\lambda_0 \times 0.005\lambda_0$ at 1 GHz PHS: $40 \times 35 \times 1.6 \text{ mm}^3$	0.41–4.1 GHz (165.84%)	4.45 dBi	85.8%
---------------------	--	------------------------	----------	-------

III. CONCLUSIONS

The feasibility of a planar antenna has been demonstrated using periodic array of E-shaped complementary artificial magnetic conductor unit-cells to realize small antennas that exhibit good radiation properties in the frequency range encompassing UHF to C-band. The antenna was optimized and the finalized antenna operates over 0.41 GHz – 4.1 GHz; thus enabling communication with multiband multimode wireless communication systems. Realizing an antenna that operates across a large frequency span is normally challenging with very small antennas especially at the lower frequency boundary. The measured gain and radiation efficiency of the proposed antenna at 410 MHz is 1.05 dBi and 32.5%, respectively. The antenna has fractional bandwidth of 165.84%, peak gain and radiation efficiency of 4.45 dBi and 85.8 %, respectively, at the fifth resonance frequency of 2.76 GHz. The antenna has an overall size of $0.054\lambda_0 \times 0.047\lambda_0 \times 0.0021\lambda_0$ at 410 MHz or $40 \times 35 \times 1.6 \text{ mm}^3$. The planar nature of antenna enables easy integration with wireless transceivers.

REFERENCES

- [1] H. Laure, M. Koubeissi, M. Mouhamadou, E. Arnaud, C. Decroze and T. Monediere, “Compact and multiband dielectric resonator antenna with pattern diversity for multistandard mobile handheld devices,” *IEEE Transaction on antennas and propagation*, vol. 59, 2011, pp. 4201–4208.
- [2] J. Anguera, G. Font, C. Puente, C. Borja and J. Soler, “Multifrequency microstrip patch antenna using multiple stacked elements,” *IEEE microwave and wireless components letters*, vol. 13, 2003, pp. 123–124.
- [3] J. H. Yoon, Y. C. Rhee, Y. K. Jang, “Compact monopole antenna design for WLAN / WiMAX triple-band operations,” *Microwave and Optical. Tech. Lett.*, vol. 54, 2012, pp. 1838–1846.
- [4] J. Won-Gyu and J.-H. Choi, “Design of a wide and multiband aperture-stacked patch antenna with reflector,” *Microwave and optical technology letters*, vol. 49, 2007, pp. 2822–2824.
- [5] J. Anguera, A. Andújar, M.C. Huynh, C. Orlenius, C. Picher, C. Puente, “Advances in antenna technology for wireless handheld devices”, *Int. Journal of Antenna and Propagation*, 2013.
- [6] C. Caloz and T. Itoh, *Electromagnetic Metamaterials: Transmission Line Theory and Microwave Applications*. New York: Wiley, 2006.

- [7] M. Alibakhshi-Kenari, M. Naser-Moghadasi and R. A. Sadeghzadah, "Bandwidth and radiation specifications enhancement of monopole antennas loaded with split ring resonators," *IET Microwaves, Antennas & Propagation*, vol. 9, issue 14, 19 November 2015, p. 1487 – 1496.
- [8] R. W. Ziolkowski and A. Erentok, "Metamaterial-inspired efficient electrically small antennas," *IEEE Trans. Antennas Propagat.*, vol. 56, no. 3, March 2008, pp. 691–707.
- [9] M. Alibakhshi-Kenari, M. Naser-Moghadasi, B. S. Virdee, A. Andújar and J. Anguera, "Compact antenna based on a composite right/left handed transmission line," *Microwave and Optical Technology Letters*, vol. 57, issue 8, August 2015 pp. 1785–1788.
- [10] M. Alibakhshi-Kenari, M. Naser-Moghadasi and R. A. Sadeghzadeh, "Composite RightLeft-Handed-Based Antenna with Wide Applications in Very-High Frequency–Ultra-High Frequency Bands for Radio Transceivers," *IET Microwaves, Antennas & Propagation*, vol. 9, issue 15, 10 December 2015, p. 1713 – 1726.
- [11] M. Alibakhshi-Kenari, "Introducing the new wideband small plate antennas with engraved voids to form new geometries based on CRLH MTM-TLs for wireless applications," *International Journal of Microwave and Wireless Technologies*, vol. 6, special issue 6, Dec. 2014, pp 629 – 637.
- [12] M. Alibakhshi-Kenari and M. Naser-Moghadasi, "Novel UWB miniaturized integrated antenna based on CRLH metamaterial transmission lines," *AEU – Int. Journal of Electronics and Communications*, vol. 69, issue 8, August 2015, pp. 1143–1149.
- [13] M. A. Antoniadis and G. V. Eleftheriades, "A CPS leaky-wave antenna with reduced beam squinting using NRI-TL metamaterials," *IEEE Trans. Antennas Propagat.*, vol. 56, no. 3, March 2008, pp. 708–721.
- [14] M. A. Y. Abdalla, K. Phang, and G. V. Eleftheriades, "A steerable series-fed phased array architecture using tunable PRI/NRI phase shifters," *Int. Workshop on Antenna Technology: Small Antennas and Novel Metamaterials*, Japan, 2008, pp. 83–86.
- [15] G. V. Trentini, "Partially reflecting sheet arrays," *IEEE Trans. Antennas Propag.*, vol. AP-4, 1956, pp. 666–671.
- [16] G. Goussetis, Y. Guo, A. P. Feresidis and J. C. Vardaxoglou, "Miniaturized and multi-band artificial magnetic conductors and electromagnetic band gap surfaces," *IEEE Antennas Propagation Society Int. Symp.*, 20-25 June 2004, vol. 1, pp. 293–296.
- [17] M. A. Hiranandani, A. B. Yakovlev and A. A. Kishk, "Artificial magnetic conductors realised by frequency-selective surfaces on a grounded dielectric slab for antenna applications," *IEE Proc.-Microw. Antennas Propag.*, vol. 153, no. 5, October 2006, pp. 487–493.
- [18] Zhijun Zhang, *Antenna Measurement*, Wiley-IEEE Press, March 2011.

- [19] J. Luo, S. Gong, P. Duan, C. Mou, and M. Long, "Small-Size Wideband Monopole Antenna with CRLH-TL for LTE Mobile Phone," *Progress In Electromagnetics Research C*, vol. 50, pp. 171–179, 2014.
- [20] M. A. Abdalla, A.A. Awad, K.M. Hassan, "Wide Band High Selective Compact Metamaterial Antenna for 2 GHz Wireless Applications," *Antennas and Propagation Conf. (LAPC)*, pp. 350–354, Nov. 2014.
- [21] Y. Li, Z. Zhang, J. Zheng and Z. Feng, "Compact heptaband reconfigurable loop antenna for mobile handset," *IEEE Antennas and Wireless Propagation Letters*, vol. 10, pp. 1162–1165, 2011.
- [22] C. J. Lee, K. M. K. H. Leong, T. Itoh, "Composite right/left-handed transmission line based compact resonant antennas for RF module integration," *IEEE Trans. Antennas Propag.*, vol. 54, no. 8, pp. 2283–2291, 2006.
- [23] C. J. Lee, K. M. H. Leong, and T. Itoh, "Broadband small antenna for portable wireless application," *International Workshop on Antenna Technology: Small Antennas and Novel Metamaterials, iWAT 2008*, pp. 10–13, 2008.
- [24] C.-C. Yu, M.-H. Huang, L.-K. Lin, Y.-T. Chang, "A compact antenna based on MTM for WiMAX," *Asia-Pacific Microwave Conference, (APMC)*, Macau-China, Dec. 2008.